JOURNAL OF MECHANICS IN MEDICINE AND BIOLOGY
(Publisher: World Scientific)

ISSN (print): 0219-5194 | ISSN (online): 1793-6810

Accepted July 28th 2021

COMPUTATIONAL FLUID DYNAMICS SIMULATION AND VISUALIZATION OF NEWTONIAN AND NON-NEWTONIAN TRANSPORT IN A PERISTALTIC MICRO-PUMP

Mohamed El Gendy[1^], O. Anwar Bég[2*], A. Kadir[2], M.N. Islam [3] and D. Tripathi [4]

[1]Lufthansa Technik Malta (LTM), Malta Intl. Airport Hal Farrug Road Luqa LQA 3079 ***Malta****.*

[2]Department of Aeronautical and Mechanical Engineering, School of Science, Engineering and Environment, University of Salford, Newton Building, Manchester, M54WT, ***UK****.*

[3]Computational Mechanics, Aerospace Engineering, Sheffield Hallam University, S11WB, ***UK.***

[4]Department of Mechanical Engineering, Manipal University Jaipur, Rajasthan-303007, ***India.***

ABSTRACT

Motivated by recent developments in bio-inspired medical engineering microscale pumps, in the present article a 3-dimensional sequential simulation of a peristaltic micro-pump is described to provide deeper insight into the hydromechanics of laminar, viscous flow in peristaltic propulsion. The Carreau and power-law models are employed for non-Newtonian behavior. The commercial software package ANSYS Fluent is utilized to conduct a numerical simulation of laminar peristaltic pump fluid dynamics, based on the finite volume method and steady space laminar solver. Details are provided for the geometric pump design (conducted with AUTOCAD), pre-processing (meshing) and necessary boundary conditions to simulate the peristaltic flow within the pump. Extensive visualization of velocity, pressure and vorticity contours is included. The present simulations provide a benchmark for future comparison with experimental studies and indeed more advanced numerical simulations with alternative non-Newtonian models. Applications of the study include biomimetic blood flow pumps, blood dialysis machines, microscale infusion pumps etc.

KEY WORDS: *Peristaltic micro-pumps; CFD; flow visualization; Vorticity; Carreau and power-law model.*

*****Corresponding author- email: O.A.Beg@salford.ac.uk; gortoab@gmail.com.*

^Now at Alkan Medical, Cairo, Egypt.

NOTATION

Times new Roman

g is gravitational acceleration (m/s^2)

n is exponent (power law) index in both Ostwald-DeWaele and Carreau models (no units)

p is pressure (Pa)

t is time (s)

u,v,w are the velocities in the (x,y,z) coordinate directions respectively (m/s)

Greek

ρ is fluid density (kg/m^3)

μ is dynamic (Newtonian) viscosity (Pa· s),

μ_0 is the zero shear rate viscosity in Carreau model (Pa· s),

μ_∞ is the infinite shear rate viscosity Carreau model (Pa· s),

λ is the relaxation time (s)

$\dot{\gamma}$ is shear rate in both power-law and Carreau model (s^{-1})

μ_0 * is the flow consistency index in power-law model (Pa· s),

1. INTRODUCTION

Bio-inspired micro-pump design in medical engineering has witnessed significant interest in recent years [1]. Many sophisticated mechanisms arise in nature which can be mimicked to improve the efficiency and robustness of industrial micro-pumps. These include ciliated walls, variable stiffness and wall deformability, adaptive healing, surface tension, electro-osmosis and many other intriguing features. One of the most efficient and frequently deployed mechanisms of biological transport is *peristalsis*. Peristalsis involves the propulsion of physiological fluids via rhythmic contraction of the walls of a vessel. It arises in phloem translocation in botany, embryonic heart development, blood transport in narrow vessels and intestinal dynamics. Numerous studies of peristaltic pumps have been communicated in recent years [2-6]. The majority of computational and analytical studies which address peristaltic pumping flows have used Newtonian models and have been restricted to 2-dimensional simulations employing lubrication theory. Interesting Newtonian peristaltic analyses include Tsui *et al.* [7], Kothandapani and Srinivas [8], Kumar *et al.* [9], Jimenez-Lozano and Sen [10]

and Reddy *et al*. [11]. These studies have addressed both tube and channel geometries with deformable conduit walls. Most physiological fluids including blood however exhibit non-Newtonian properties which manifest as deformation-rate dependency, yield stress, viscoelasticity, thixotropy. The high concentration of suspended particles (red blood cells, proteins, nutrients, leukocytes) and their inherent elasticity contribute strongly to non-Newtonian behavior, especially in narrow vessels (micro-circulation). Non-Newtonian effects are therefore also likely to contribute strongly in blood micro-pump dynamics even at low deformation rates [12]. Many researchers have therefore employed a range of non-Newtonian (bio-rheological) models to simulate peristaltic flows of blood and other biological fluids. These studies include Muthu *et al.* [13] who considered micropolar fluid theory (to represent spin of suspended particles). Tripathi *et al.* [14] utilized a Nakamura-Sawada bi-viscosity model to study peristaltic pumping in a curved conduit. Shafie *et al*. [15] studied heat transfer in peristaltic flow of Sisko fluids with cross-diffusion effects, examining both shear-thinning and thickening effects. Tripathi and Bég [16] presented a detailed study of a variety of viscoplastic biofluids propelled by peristaltic waves, including the Casson model, Herschel-Bulkley Vocadlo models. Viscoelastic fluid peristaltic propulsion has also been studied using the Reiner-Rivlin third order model by Ali *et al.* [17] (who also examined wall slip) and the Jefferys model by Tripathi *et al.* [18] who also considered electro-osmotic and finite conduit length effects. A simple but popular model in non-Newtonian fluid mechanics is the Ostwald-DeWaele power-law model. This allows deviations from the non-Newtonian model via a power law index for the shear rate and includes both dilatant (shear-thickening i.e. viscosity is elevated under increasing shear strain and power-law index exceeds unity) and pseudo-plastic (shear-thinning i.e. viscosity reduces under increasing shear strain and power-law index is less than unity) fluids, the latter being more appropriate for blood flows. Several studies of power-law peristaltic hydrodynamics have been comunicated including the articles of Rao and Mishra

[19] and Hina *et al.* [20]. Reddy *et al.* [21] also studied power-law channel flow under peristaltic waves with the same speed but different amplitudes and phases on the flexible walls of the channel, presenting extensive solutions for the influence of power-law rheological index on pumping characteristics and axial velocity distributions. Another relatively simple non-Newtonian model is the Carreau fluid which also exhibits shear-rate dependent viscosity. An interesting feature of this model is that it degenerates to the Newtonian viscous fluid at small shear rates and behaves as a power-law fluid at large shear rates. Sobh [22] investigated using a perturbation method the peristaltic pumping of a Carreau fluid in an asymmetric channel, describing the influence of Weissenberg number and wall slip on the axial velocity and pressure gradient. Ali *et al*. [23] used a finite difference numerical method to simulate the peristaltic transport of a Carreau fluid in a curved channel under the long wavelength and low Reynolds number assumptions, noting that for shear-thickening fluids, significant axial flow acceleration accompanies an increase in Weissenberg number. Further studies of Carreau fluid peristalsis and power-law peristaltic dynamics have been presented by Akram [24] and Chaube *et al.* [25], respectively. The above studies have generally utilized numerical methods to solve dimensionless models under lubrication approximations. This approach severely limits the applicability of these models to actual engineering and clinical applications. Modern computational fluid dynamics (CFD) commercial softwares however provide currently the most comprehensive simulation tools for modelling real-world peristaltic flows. These tools utilize finite volume or finite element solvers. Several authors have successfully analyzed peristaltic Newtonian flows by simulating fluid structure interaction (FSI) between the propelled fluid and the deformable walls. Kozu *et al.* [26] used a commercial CFD code to analyze the two-dimensional intra-gastric peristaltic flow and mass transfer a gastric digestive enzyme (pepsin) generated by an antral contraction wave (ACW) along the walls of the distal stomach. Vahidi and Fatouraee [27] presented a two-dimensional ureteral laminar peristaltic

simulation employing a hyperelastic, isotropic, incompressible and homogeneous material model for the wall and the ADINA finite element code with solid elements for large displacement for the wall structure, and planar fluid element for the urine flow. Najafi *et al*. [28] employed the ANSYS FLUENT finite volume code to analyze the dynamics of kidney stone displacement in ureteral peristalsis, visualizing extensively the influence of stone shape on bolus dynamics, velocity distributions, mass flow rates, pressure gradients, and wall shear stresses.

The above CFD peristaltic flow simulations were all restricted to Newtonian viscous fluids and did not consider applications in bio-inspired peristaltic micro-pumps. In the present article, 3-dimensional simulations of both Newtonian and non-Newtonian fluids in a peristaltic blood micro-pump are described. The Carreau and power-law models are deployed to characterize rheological behaviour. ANSYS Fluent [29] is implemented for the simulations. Contour plots for velocity, pressure and vorticity are incorporated. The current work is relevant to providing more realistic numerical simulations of actual peristaltic propulsion hydromechanics in bio-inspired micro-pumps [30] and it is envisaged that it will provide a useful compliment to experimental studies [2] and more elaborate non-Newtonian simulations.

2. GEOMETRIC MODEL

Utilizing the modified design of a peristaltic micro pump produced by Rishi Kant *et. al* [2] a three-dimensional model was constructed using the 3D design software AutoCAD. The outline of the model from the original study was traced and a three-dimensional copy of the domain was formed. Comparison between the original design and the traced model can be seen in Figs. 1 and 2, while Fig 3 displays the geometry produced on AutoCAD. The domain of peristaltic pump model was 9 mm in length and 2 mm in width. The height of the tube leading to the

pump outlets measured at 0.2 mm. This geometrical model was imported to ANSYS Fluent Software and the material specifications on the layers were defined. The design was further improved to include an inlet layer of 0.2 mm width to represent the pump inlet surface (Fig. 3).

3. MATHEMATICAL FLOW MODEL

Laminar, viscous dominated peristaltic flow is considered in the geometrical micro=pump domain described in Section 2. The fundamental equations for mass and momentum conservation employed in ANSYS FLUENT are the 3-D unsteady incompressible Navier-Stokes equations which comprise the *mass conservation* and *x-, y- and z-momentum* conservation equations. These may be stated as follows [29, 30]:

D'Alembert mass conservation (3-D continuity)

$$\left[\frac{\partial u}{\partial x} + \frac{\partial v}{\partial y} + \frac{\partial w}{\partial z} \right] = 0 \tag{1}$$

X-direction momentum conservation

$$\rho\left[\frac{\partial u}{\partial t} + u\frac{\partial u}{\partial x} + v\frac{\partial u}{\partial y} + w\frac{\partial u}{\partial z} \right] = \rho F_x - \frac{\partial p}{\partial x} + \mu\left[\frac{\partial^2 u}{\partial x^2} + \frac{\partial^2 u}{\partial y^2} + \frac{\partial^2 u}{\partial z^2} \right] \tag{2}$$

Y-direction momentum conservation

$$\rho\left[\frac{\partial v}{\partial t} + u\frac{\partial v}{\partial x} + v\frac{\partial v}{\partial y} + w\frac{\partial v}{\partial z} \right] = \rho F_y - \frac{\partial p}{\partial y} + \mu\left[\frac{\partial^2 v}{\partial x^2} + \frac{\partial^2 v}{\partial y^2} + \frac{\partial^2 v}{\partial z^2} \right] \tag{3}$$

Z-direction momentum conservation

$$\rho\left[\frac{\partial w}{\partial t} + u\frac{\partial w}{\partial x} + v\frac{\partial w}{\partial y} + w\frac{\partial w}{\partial z} \right] = \rho F_z - \frac{\partial p}{\partial z} + \mu\left[\frac{\partial^2 w}{\partial x^2} + \frac{\partial^2 w}{\partial y^2} + \frac{\partial^2 w}{\partial z^2} \right] \tag{4}$$

Where (u,v,w) are the velocities in the (x,y,z) coordinate directions respectively, p is pressure, F_x,F_y,F_z are the body forces (gravitational, magnetic, electrical etc), ρ is fluid density, μ is

dynamic viscosity, *t* is time. The eqns. (1)-(4) are employed in the Newtonian flow simulations. For the non-Newtonian flow simulations, both power-law and Carreau models are utilized, as defined in ANSYS FLUENT [29] with a modified viscosity formulation. The simulations are described in Secn. 6. Based on the experimental data used by Rishi Kant *et al.* (2012), the inlet was specified as pressure-inlet type zone with and both outlets as a pressure-outlet zone with a target mass flow rate specified accordingly. The temperature influence was neglect as the energy equation solver was turned off. A summary of the boundary conditions used in the simulations can be found in **Table 1** below. The viscosity in eqns (2)-(4) is modified for both the non-Newtonian Carreau model and the power-law model. The Carreau viscosity-shear rate relation as given in ANSYS Fluent [29] takes the form:

$$\mu = \mu_{\infty} + \left(\mu_0 - \mu_{\infty}\right)[1 + (\lambda\dot{\gamma})^2]^{\frac{n-1}{2}} \tag{5}$$

Here μ_0 is the zero shear rate viscosity ($= 0.056\ Pa \cdot s$), μ_{∞} is the infinite shear rate viscosity ($0.00345\ Pa \cdot s$), λ is the relaxation time (=3.313s), $\dot{\gamma}$ is shear rate (s^{-1}) which is variable and *n* is power law index (= 0.3568). The values of the parameters as used in the ANSYS simulations are given in brackets and taken from Gijsen *et al.* [31] and Robertson *et al.* [32]. The power-law model formulation for viscosity-shear rate takes the form [29]:

$$\mu = \mu_0 * (\dot{\gamma})^{n-1} \tag{6}$$

Here μ_0 * is the flow consistency index (= 0.035 Pa·s), $\dot{\gamma}$ is shear rate (s^{-1}) which is variable and *n* is power law index (= 0.6 i.e. pseudo-plastic). We further note that for the Newtonian simulations, blood has a constant viscosity of $\mu = 0.0035\ Pa \cdot s$.

4. FINITE VOLUME MESHING, PRESSURE-BASED SOLUTION, CONVERGENCE AND GRID INDEPENDENCE

A body-sizing meshing approach, compromising mainly of tetrahedron cells to accommodate the anomalous structure of the model, was used to produce an adequate meshing that satisfies the problem specifications. Refinements concentrated at the edges of the inlet and outlets where placed to resolve the complex flow in these zones. The smallest elements were situated at the walls to accommodate boundary layer conditions. The cell distribution around the model can be seen in **Figs. 5 and 6** below. Additionally, refined meshes for the domains were employed to investigate the influence of mesh size on the results for the grid independency study conducted below in **Table 2** and **Fig. 7**. The results of the grid independency study clearly shows that the values for the outflow velocity stabilizes at around 330,000 elements, with a slight difference in values after that. Thus making the original mesh the ideal choice in this situation. The simulations were conducted with the pressure based solver due to the incompressible assumption for blood [29]. The pressure-based solver relies on two types of algorithms, a segregated algorithm and a coupled one. The segregated algorithm uses sequential steps to solve the governing equations in a more memory efficient manner by storing the discretized equations once in the memory. The coupled solve solves the governing equations by coupling them together resulting in a delay in convergence and requiring more memory. Convergence is critical to achieving fast, accurate solutions. Monitoring of the regulated equation residuals of the momentum and continuity equations should preferably be lower than 10^{-5}. However, this criterion alone does not guarantee the effective validity of results. Some of the cases might not fulfill the required residual criterion regardless of the validity of the results, and other cases might yield incorrect solutions even with low residuals. Thus, the monitoring of the mass, conservation and output pressure is required. The total fractional difference between the inward and outward mass flow of the domain should ideally be below 0.01 %, while the outlet pressure and mass flow through open boundaries should remain constant for a number of iterations before settling for convergence. Furthermore

validation of the ANSYS Fluent simulations confirms the accuracy of the computations. Validation of the results can be achieved via three mechanisms- with previous theoretical, experimental or analytical work. This step guarantees the reliability of the model, where failure might lead to the need to re-assess and further modify the model to achieve optimal results. In the present study, results of the modified peristaltic micro-pump simulation are compared with the experimental work of Rishi Kant *et al.* [2].**Table 3** below shows the experimental results for the flow rate versus the actuating pressure for the optimized design peristaltic micro pump. The values were converted to accommodate the ANSYS fluent parameter requirements and the simulation was conducted for each actuating pressure factor to verify the simulative reliability. Excellent verification of solutions is demonstrated in Table 3. Confidence in the present ANSYS Fluent results is therefore justifiably high.

5. SIMULATIONS

3-D peristaltic flow simulations were conducted in ANSYS Fluent – first for two Newtonian cases (water and blood) and secondly for the two non-Newtonian blood cases. Blood was assumed to have constant density of 1050 kg/m^3 [32]. The simulations utilized the steady space laminar solver with a constant viscosity for the Newtonian behavior. Viscosity variation was incorporated with ANSYS Fluent definer functions for the non-Newtonian behavior for the Power Law and the Carreau solver models. The first part of the experiment involved simulating the fluid flow through the optimized peristaltic pump design. Water was also used for testing simulations to emulate the experimental conditions set by Kant *et al.* [2]. Their experimental study involved pumping a water solution containing fluorescent microbeads through an optimized chamber design assembly. A steady space pressure solver, coupled with a viscous laminar model, was deemed suitable for this investigation. All current simulations have been performed using a Lenovo Y510p laptop machine with 8 GB of RAM and an Intel® Core i7-4700MQ CPU @ 2.4 GHz processor with a NVidia® 755m gt SLI GPU running on a Windows

10 platform. The solver was set to include double precision option to allow a higher rate of accuracy and parallel processing option was enabled to utilize the power of the multi core system and the double GPU feature within the machine. The effect of gravity was also taken into consideration with g = -9.81 m/s^2 along the z-axis. First the velocity distribution along the length of the micro channel was computed. Next the pressure distribution was computed. In addition the vorticity was also computed at specified regions of action around the design of the micro pump. All of the distributions presented were taken along half of the length of the microchannel due to the symmetrical nature of the results on both sides. The visualizations to be described include 4 cases: water, Newtonian blood, and two non-Newtonian models for blood in peristaltic propulsion.

5.1 Velocity Distribution along the Micro pump

The velocity distribution along the micro-pump for all the 4 cases are plotted in **Figs. 8-11**. Velocity contours for each case were also visualized and are presented in **Figs. 12-15**. Figure 16 furthermore summarizes the above plots to provide an easy means of comparison. All cases follow the same trend as the fluid flows from the inlet toward the outlet. They exhibit a sigmoidal velocity growth which is characteristic of micro-pumps [3, 4]. An inlet velocity of 0.2 at the inlet induces a small spike in the velocity profile across the four micro pumps that moves at a steady rate towards the outflow pump at 0.75 mms from the inlet. The micro pump design allows the emulation of the peristaltic action that propels the fluid from the main chamber towards the outlet by the rhythmic contraction of the pump chamber walls. This action induces a large spike in velocity as the fluid moves through the outflow pipe as can be seen in figure 16 above. The highest spike is associated with the non-Newtonian blood flow simulated by the Carreau model as the velocity increased to value of approximately 1.8 m/s. The power law model of the non-Newtonian blood flow showed a similar rate of increase as the Carreau model. However the spike settled at a lower velocity of approximately 1.3 m/s. Newtonian

blood flow, interestingly, showed a comparable velocity profile to that of the non-Newtonian power law model reaching velocities of 1.3 m/s, however, at a slightly lower flowrate. As expected the trend lines for both Newtonian flows showed close correlation with an almost identical trend as the fluid reaches the outflow pump. The much lower viscosity of water allowed the attainment of significantly higher velocity magnitudes. The relatively low viscosity of water also enables it to achieve a steady rise in velocity (flow acceleration) as it progresses through the distensible tube, reaching velocities of 1.795 m/s. The simulations confirm the potential of using peristaltic pumping as an efficient mechanism for transportation of both low and high viscosity fluids. Backflow is eliminated and steady flow profiles are generally maintained along the length of the micro-channel. The results also demonstrate the deviation in response (and hydro-mechanical pumping efficiency) between the power law model and the Carreau model, with the latter attaining more realistic values. The non-Newtonian property of blood i.e. shear thinning, leads to a drop in viscosity. This drop in viscosity is due to the increase in shear strain observed when the fluid moves from the main chamber towards the outflow pipe. This behavior is not seen in Newtonian fluids and thus explains the average rise in speed observed above for the non-Newtonian cases. The figures provide a clear visual representation of the fluid dynamics of 3-D peristaltic pumping.

5.2 Pressure Distributions along the Micro Pump

We now consider the pressure and pressure contour distributions for all 4 cases produced through the ANSYS Fluent simulations. As can be seen above from the pressure distribution plots, **Figures 17-20**, there are clear distinguishing factors between the Newtonian and non-Newtonian models. The first two Newtonian models showed very similar trends with high pressure regions being observed in the chamber area and a steady sharp decline as the fluid is pumped out of the microchannel. This can be attributed to the viscosity profile of the Newtonian fluids. The water model showed a higher starting pressure that undergoes a drop in

magnitude from $1.84e^5$ Pa to approximately $1.81e^5$ Pa. However the Newtonian blood model achieved lower pressure levels due to its higher viscos nature with a starting pressure of $8.3e^4$ Pa dropping at a higher rate to $7.5e^4$ Pa. The shear thinning behavior, commonly seen in non-Newtonian fluids, results in magnitudes of pressure which deviate significantly from those computed for Newtonian fluids. The starting pressure for both the power law model and the Carreau model remained high at 8.3e4 Pa and ascended up to $8.95e^4$ Pa for the power law model and $9.13e^4$ for the Carreau model. This once again proved the efficiency of the Carreau model over the Power Law model for peristaltic pumping. Visualization of all four cases can be seen in **Figures 21-24**. The trapped bolus is clearly visualized again in these plots.

5.3 *Vorticity Distribution along Micro-Pump*

This section outline the vorticity distribution plots and contours for all cases produced through the simulation. Vorticity allows an appreciation of the tendency of a fluid particle to rotate or circulate at a particular point. It also contributes strongly to trapping phenomena in peristaltic fluid mechanics [33]. ANSYS Fluent allows vorticity computation easily via the "flow physics" GUI specifications [29]. **Figs. 25- 28** illustrate the vorticity distributions all 4 cases examined, namely the Newtonian cases (water and blood) and the non-Newtonian cases (power-law and Carreau). **Figs. 29-32** present the 3-D vorticity contour visualizations again for all 4 cases studied. The vorticity distribution profiles are particularly interesting for the four cases due to the varying nature of the results. We note that vorticity equals the curl of the velocity, and effectively embodies how a fluid element rotates as it travels with the main stream of flow. A small increase in vorticity at the inlet as the fluids hit the back of the chamber is evident for all the cases with water retaining the maximum vorticity at this point, reaching values of 15000 (s^{-1}) followed by a vorticity ranging from 7500 (s^{-1}) to 10000 (s^{-1}) for the remaining cases. For both Newtonian cases, the maximum vorticity was noted at the entrance of the outflow pump from the main chamber achieving values of 83000 (s^{-1}) and 50000 (s^{-1}) for the water

and blood respectively. On the other hand maximum vorticity for the non-Newtonian cases was achieved at the micro pump outlet with the power model achieving a modest 57500 (s^{-1}) while the Carreau model attained significantly higher vorticity of 85000 (s^{-1}).

6. CONCLUSIONS

A 3-D computational fluid dynamics (CFD) study has been presented to investigate the peristaltic transport on Newtonian and non-Newtonian fluids along an optimized micro-pump channel. The micro-pump design is based on previous experimental investigations and has been computationally rendered using AutoCAD software. The geometric micro-pump model has then been imported into the ANSYS Fluent (finite volume method) solver to simulate the peristaltic flow. A grid independence study has been performed to confirm adequate meshing for the solver. The solver settings were set to emulate experimental conditions and the simulation was initially tested for water pumping. The consistent validation of results allowed the progression of the study into the simulation of blood flow using both Newtonian and non-Newtonian models. Due to the large variety of existing rheological models available for non-Newtonian fluid characteristics, two simple but relatively accurate non-Newtonian models were selected, namely the Ostwald-DeWaele power law model (for pseudo-plastic shear-thinning fluids) and the more complex Carreau model. Extensive simulations were performed and detailed visualization of velocity, pressure and vorticity profiles along the length of the micro pump presented. Carreau fluid was shown to achieve the best performance and maximum pumping efficiency and indeed is the most robust of the models studied for blood simulation. The current investigation may be extended by considering more complex rheological models

(micropolar, viscoelastic) and also curvature of the pumping conduit. These will be addressed in the future.

REFERENCES

[1] Laser DJ, Santiago JG (2004) A review of micropumps. *J Micromech Microeng* 14:35

[2] Kant, R., Singh, H., Nayak, M. and Bhattacharya, S., (2013). Optimization of design and characterization of a novel micro-pumping system with peristaltic motion. *Microsystem Technologies*, 19(4), pp.563-575.

[3] Acero MC, Plaza JA, Esteve J, Carmona M, Marco S, Samitier J (1997) Design of a modular micropump based on anodic bonding. *J Micromech Microeng* 7:179–182

[4] Bohm S, Olthuis W, Bergveld P (1999) A plastic micropump constructed with conventional techniques and materials. *Sens Actuators A* 77:223–228

[5] Aboelkassem, Y., 2012. Novel bioinspired pumping models for microscale flow transport. *PhD Dissertation. Virginia Tech, Blacksburg*, VA, USA.

[6] Goulpeau J, Trouchet D, Ajdari A, Tabeling P (2005) Experimental study and modeling of polydimethylsiloxane peristaltic micropumps. *J Appl Phys* 98:044914.

[7] Tsui, YY *et al.* (2013) Pumping flow in a channel with a peristaltic wall, *ASME J. Fluids Eng.* 136(2):021202-021202-9.

[8] Kothandapani M and Srinivas S (2008) Nonlinear peristaltic transport of Newtonian fluid in an inclined asymmetric channel through a porous medium, *Phys. Lett. A*, 372**,** 1265–1276.

[9] Ravi Kumar YVK, Krishna Kumari PN, Ramana Murthy MV and Sreenadh, S. (2010), Unsteady peristaltic pumping in a finite length tube with permeable wall, *ASME J. Fluids Eng.* 2010; 132(10):101201-101201-4.

[10] Jimenez-Lozano J and Sen M (2009). Streamline topologies of two-dimensional peristaltic flow and their bifurcations, *Chem. Eng. Process.: Process Intensification***, 47**, 704.

[11] Reddy MV, Manoranjan M, Sreenadh S and Ramachandra Rao A (2005). Influence of lateral walls on peristaltic flow in a rectangular duct, *ASME J. Fluids Eng.* 127(4):824-827.

[12] Goldsmith HL and Skalak R (1975). Hemodynamics, *Ann. Rev. Fluid Mechanics,* 7: 213-247.

[13] Muthu P, Ratish Kumar BV, Chandra P (2003). On the influence of the wall properties in the peristaltic motion of micropolar fluid, *ANZIAM J* 45:246–260.

[14] D. Tripathi, N. S. Akbar, Z. H. Khan and O. Anwar Bég (2016). Peristaltic transport of bi-viscosity fluids through a curved tube: a mathematical model for intestinal flow, *Proc. IMechE-Part H: J Engineering in Medicine.* DOI. 10.1177/095441 1916658318

[15] Shafie S, Mehmood OA and Mustapha N (2013). Thermal diffusion and diffusion thermo effects on peristaltic flow of Sisko fluid in non-uniform channel with dissipative heating, *ASME J. Heat Transfer.* 2013; 135(12):122004-122004-9.

[16] D. Tripathi and O.Anwar Bég (2014). Mathematical modeling of peristaltic propulsion of viscoplastic fluids, *Proc. IMECHE- Part H; J. Engineering in Medicine, 228 (1): 67-88.*

[17] N. Ali; Y. Wang; T. Hayat; M. Oberlack (2008). Slip effects on the peristaltic flow of a third grade fluid in a circular cylindrical tube, *ASME J. Appl. Mech.,* 76(1):011006-011006-10.

[18] D. Tripathi, A. Yadav and O. Anwar Bég (2017). Electro-kinetically driven peristaltic transport of viscoelastic physiological fluids through a finite length capillary: *mathematical modelling, Mathematical Biosciences,* 283, 155-168.

[19] Ramachandra Rao A, Mishra M (2004). Peristaltic transport of a power-law fluid in a porous tube, *J Non-Newtonian Fluid Mech*., 121:163–174.

[20] Hina S, Mustafa M, Hayat T and Alsaedi A (2013). Peristaltic flow of pseudo-plastic fluid in a curved channel with wall properties, *ASME J. Appl. Mech.* 2013; 80(2):024501-024501-7.

[21] Subba Reddy MV, Ramachandra Rao A and Sreenath S (2007). Peristaltic motion of a power law fluid in an asymmetric channel, *Int. J. Nonlinear Mech*., 42**,** 1153–1161.

[22] Sobh AM (2009). Slip flow in peristaltic transport of a Carreau fluid in an asymmetric channel, *Canadian J. Physics*, 87(8): 957-965.

[23] Ali N, Javid K, Sajid M and O. Anwar Bég (2016). Numerical simulation of peristaltic flow of a biorheological fluid with shear-dependent viscosity in a curved channel, *Computer Methods in Biomechanics and Biomedical Engineering,* 19 (6) 614-627.

[24] Akram S (2014). Effects of slip and heat transfer on a peristaltic flow of a Carreau fluid in a vertical asymmetric channel, *Computational Mathematics and Mathematical Physics*, 54, 886–1902.

[25] Chaube MK, Tripathi D, Bég O Anwar, Sharma S and Pandey VS (2015). Peristaltic creeping flow of power law physiological fluids through a non-uniform channel with slip effect, *Applied Bionics and Biomechanics (2015).* Volume 2015, Article ID 152802, 10 pages. http://dx.doi.org/10.1155/2015/152802.

[26] Kozu, H., Kobayashi, I., Nakajima, M. *et al.* (2010). Analysis of flow phenomena in gastric contents induced by human gastric peristalsis using CFD, *Food Biophysics*: 330. doi:10.1007/s11483-010-9183-y

[27] Vahidi B and Fatouraee N (2007). Computational modeling of ureteral peristaltic transport using fluid structure interaction, *ASME 2007 Summer Bioengineering Conference, June 20, Keystone, Colorado, USA*

[28] Najafi Z, Gautam P; Schwartz BF, Chandy AJ and Mahajan AM (2016). Three-dimensional numerical simulations of peristaltic contractions in obstructed ureter flows, *ASME J Biomech Eng.* 2016; 138(10):101002-101002-7.

[29] ANSYS FLUENT Theory Guide (2012). *ANSYS, Inc.*, Canonsburg, USA, Release 14.5.

[30] El Gendy M (2016). Investigation of the effect of primary peristaltic transport in Newtonian and non-Newtonian fluids using an optimized micro-pump, *MSc Thesis, Aerospace Engineering*, Salford University, Manchester, UK, September.

[31] Gijsen FJH, Allanic E, van de Vosse FN and Janssen JD (1999). The influence of the non-Newtonian properties of blood on the flow in large arteries: unsteady flow in a 90 degrees curved tube, *J. Biomechanics*, 32(6):601-608.

[32] Robertson AM, Sequeira A and Owens RG (2009). Rheological models for blood, *Formaggia L, Quarteroni A, Veneziani A (Eds.): Cardiovascular Mathematics. Modeling and Simulation of the Circulatory System,* Springer-Verlag Milan, Italy.

FIGURES

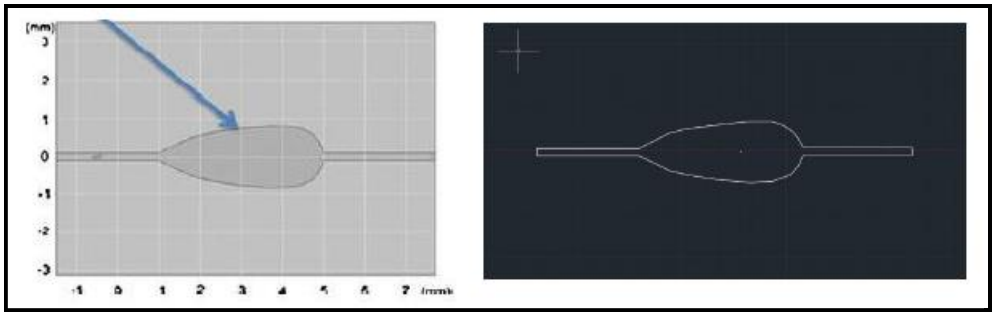

Figs. 1 and 2 Comparison between original (left) and traced (right) design

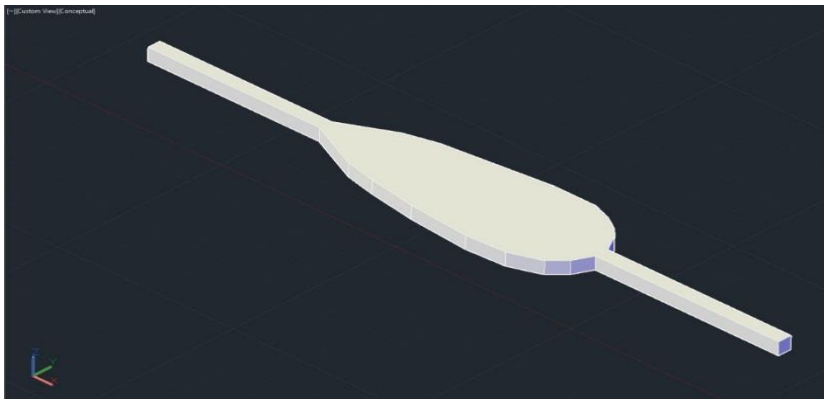

Fig. 3 Three dimensional model created on AutoCAD

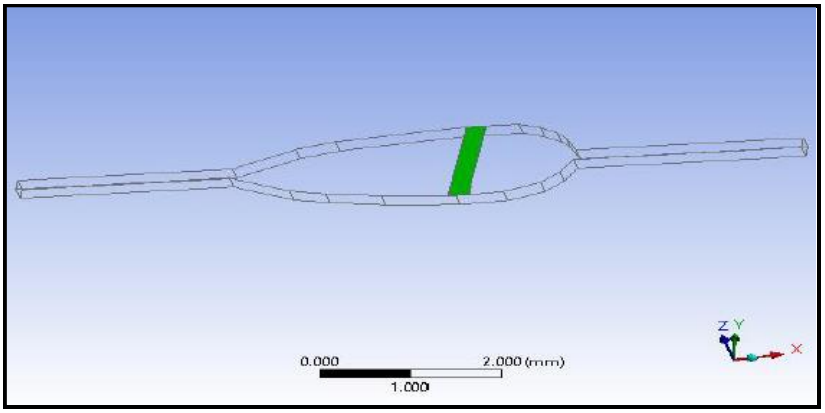

Fig. 4 Modified geometry of the model including inlet surface.

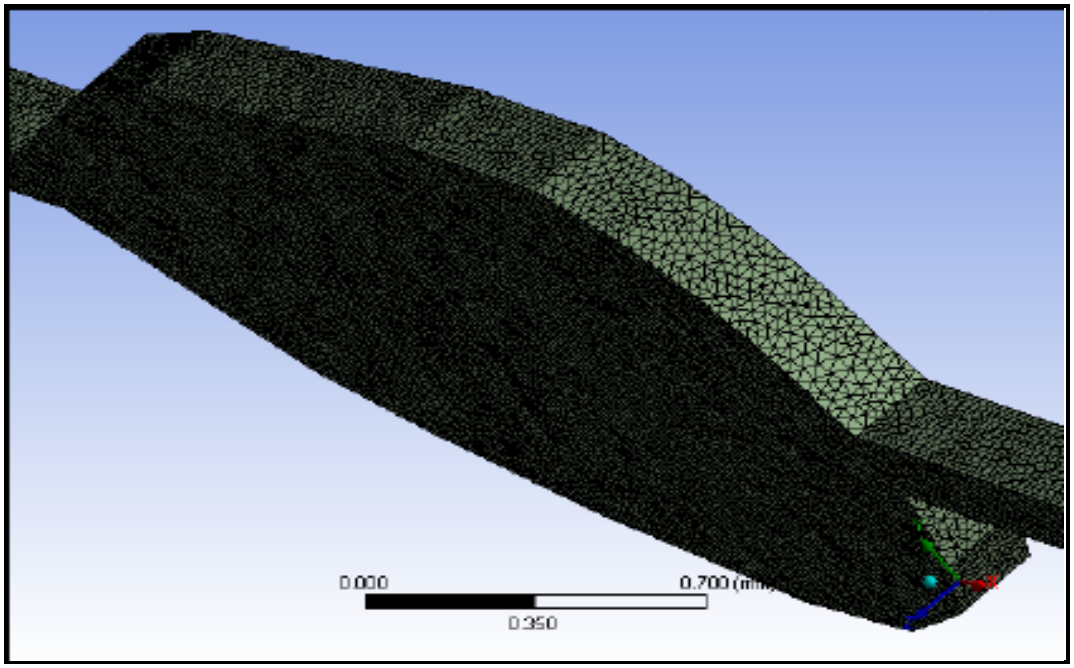

Fig. 5 Isometric top view of the model mesh indicating the inflation presented along the boundary walls

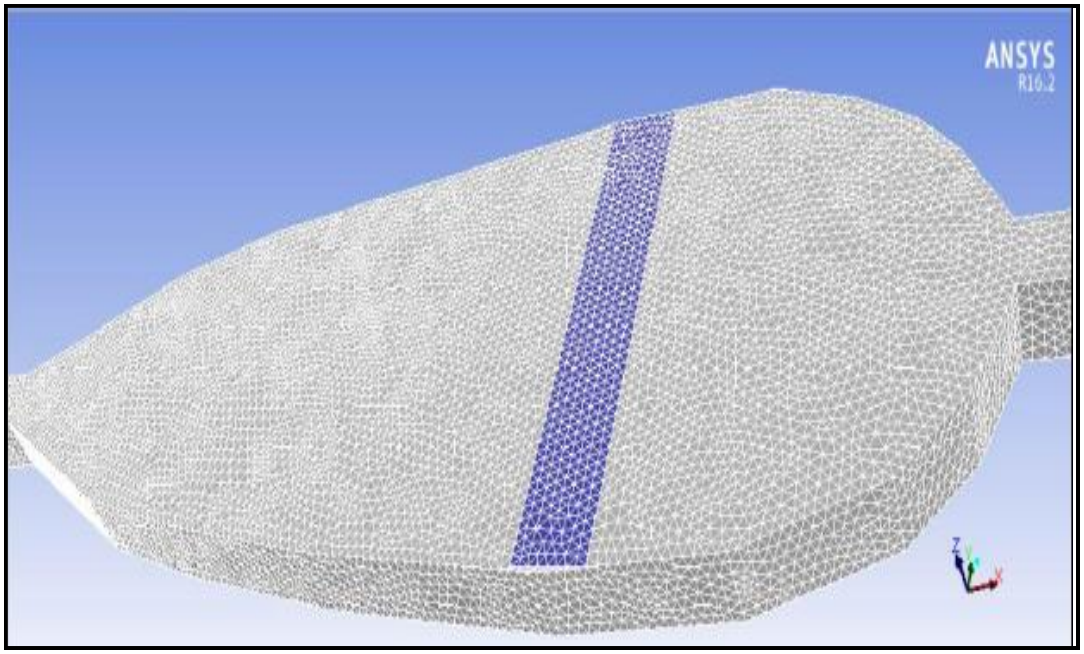

Fig. 6 isometric side view of the model mesh outline indicating the refinement along the inlet surface.

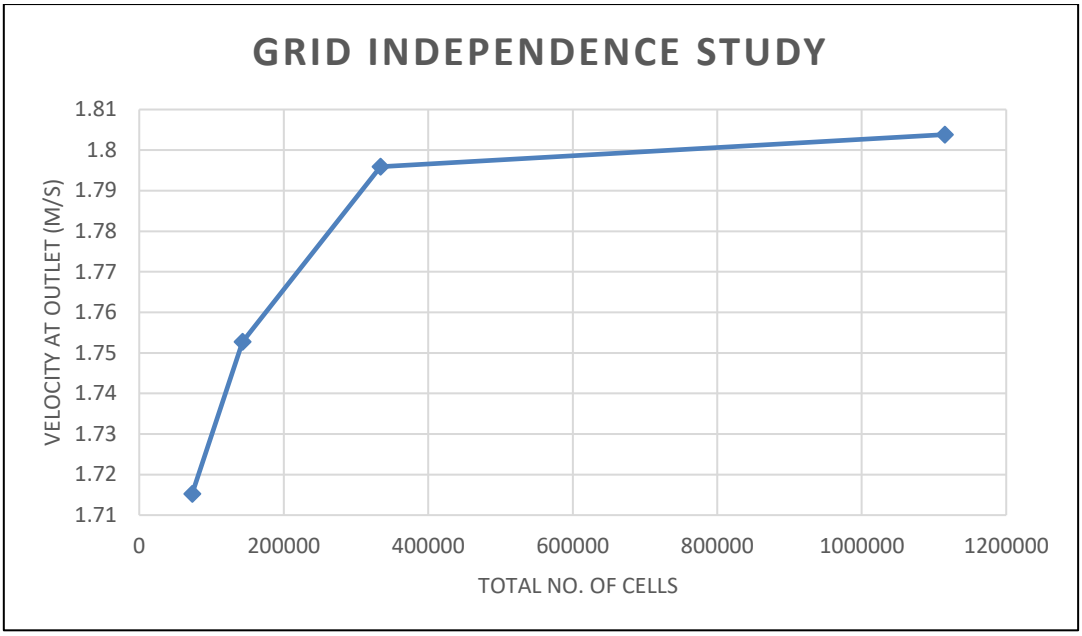

Fig 7: Grid independence study

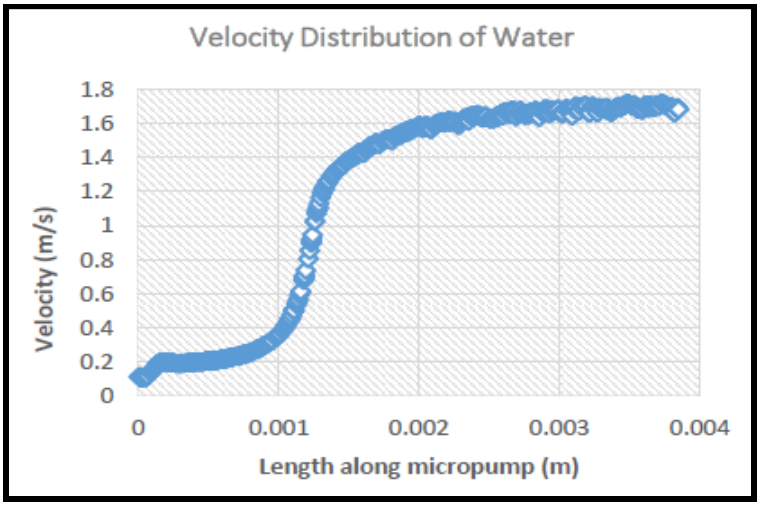

Fig. 8 Velocity plot for water (Newtonian)

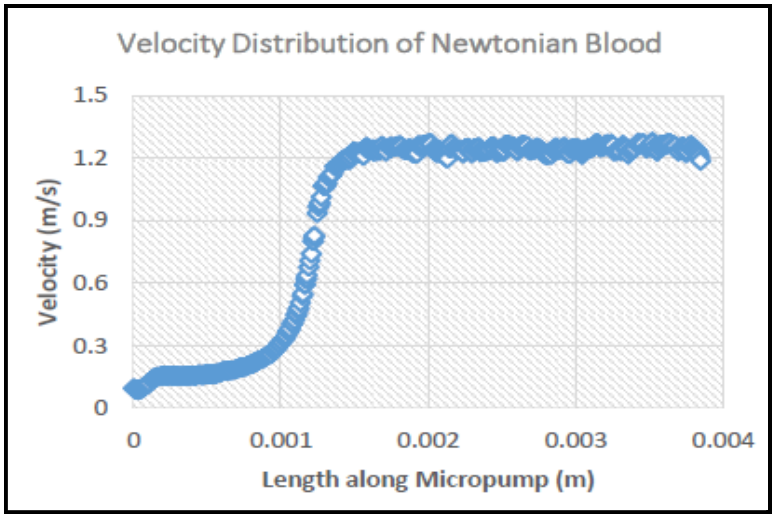

Fig. 9 Velocity plot for blood (Newtonian)

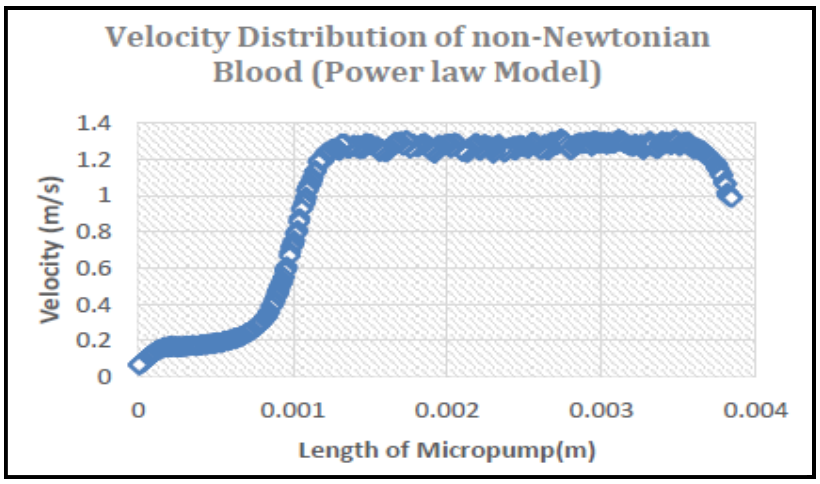

Fig. 10 Velocity plot for blood (power-law non-Newtonian)

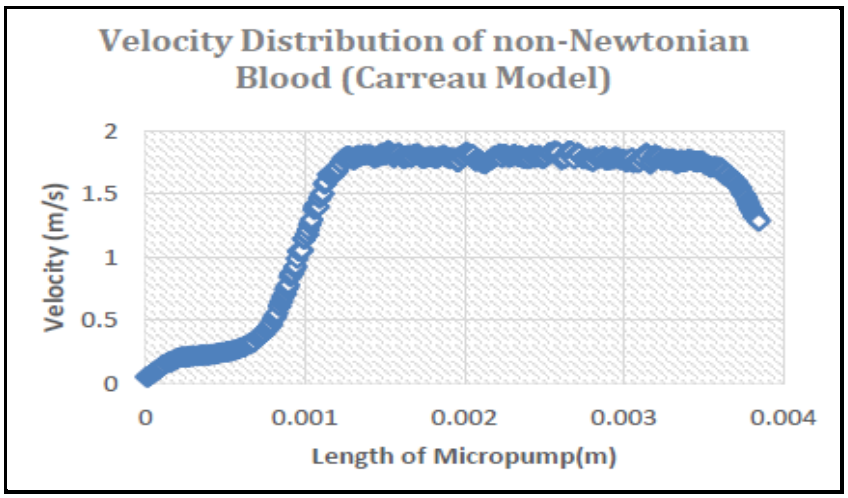

Fig. 11 Velocity plot for blood (Carreau non-Newtonian)

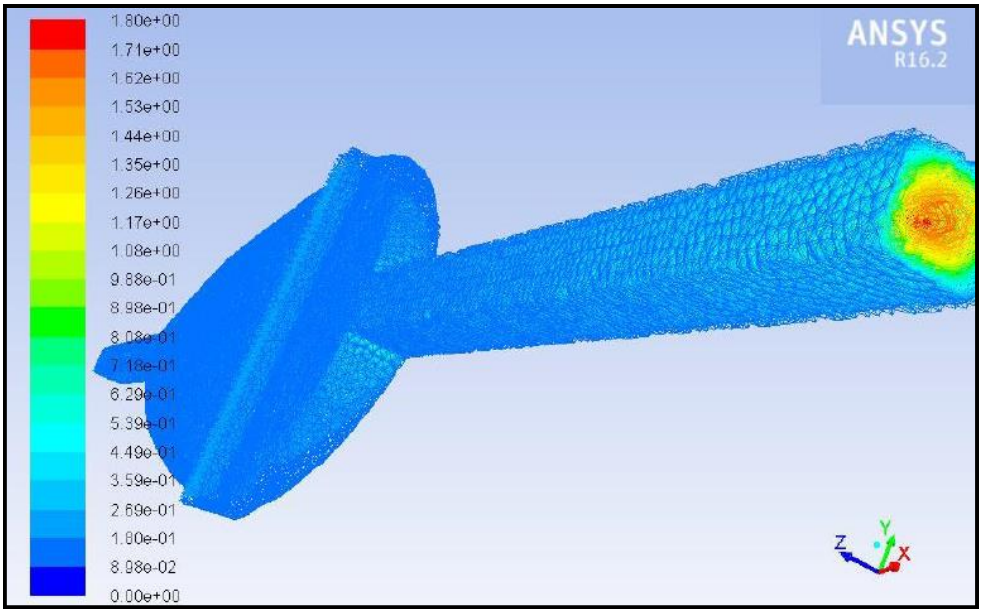

Fig. 12 3-D velocity contour plot for water (Newtonian)

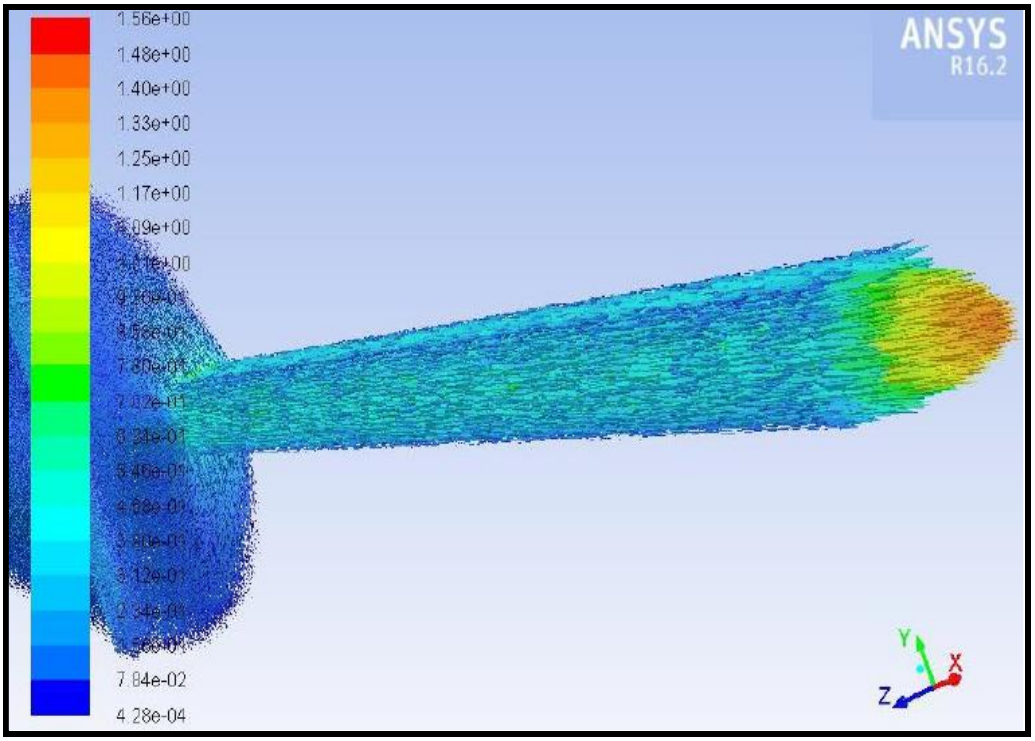

Fig. 13 3-D velocity contour plot for blood (Newtonian)

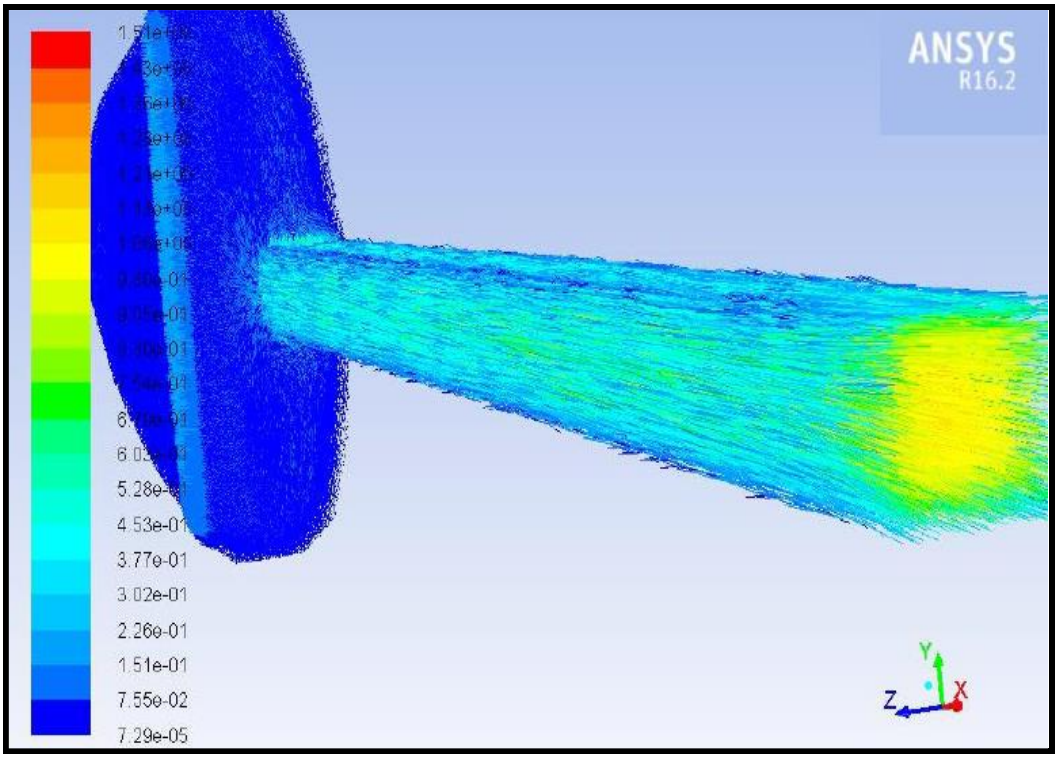

Fig. 14 3-D velocity contour plot for blood (power-law non-Newtonian)

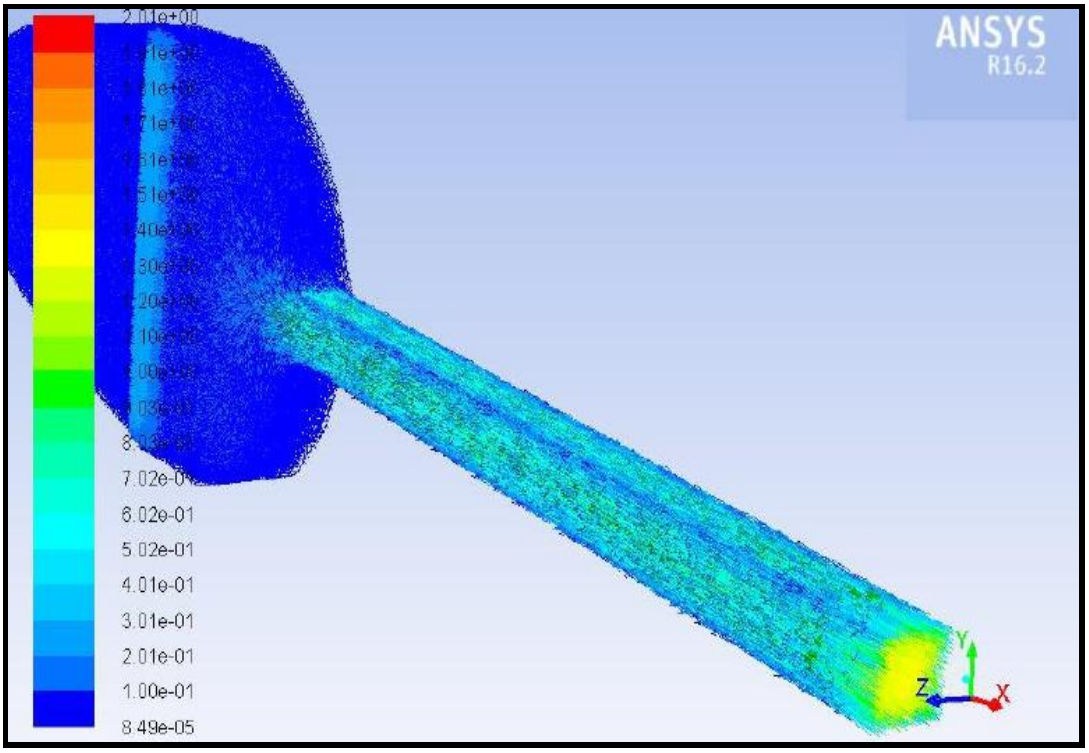

Fig. 15 3-D velocity contour plot for blood (Carreau non-Newtonian)

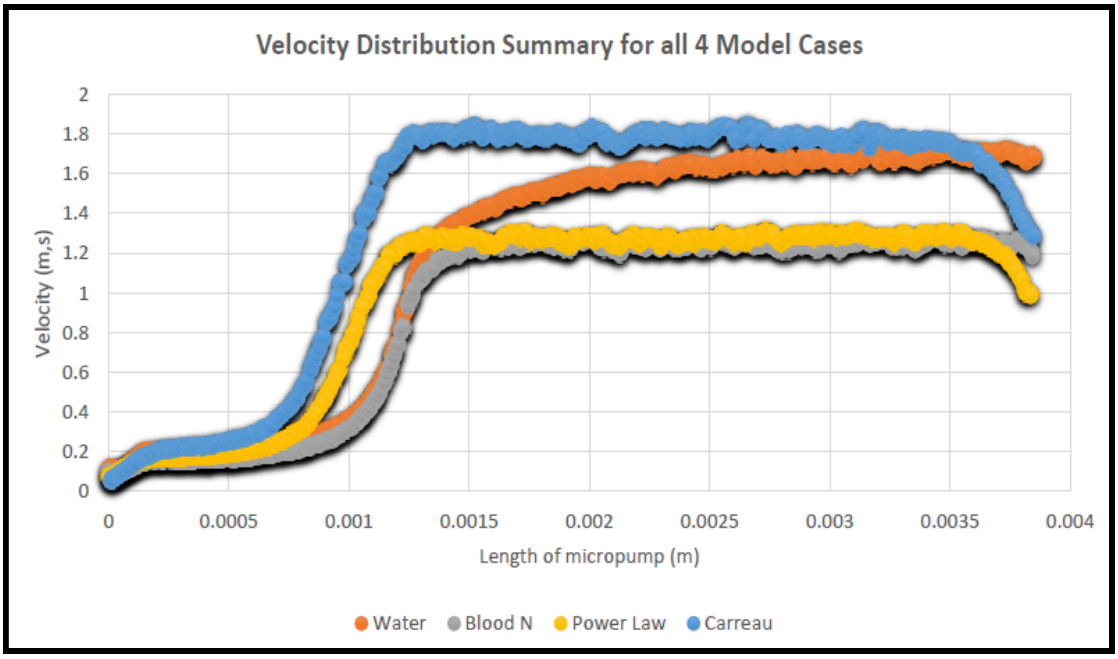

Fig. 16 Summary comparing velocity distribution for all 4 cases

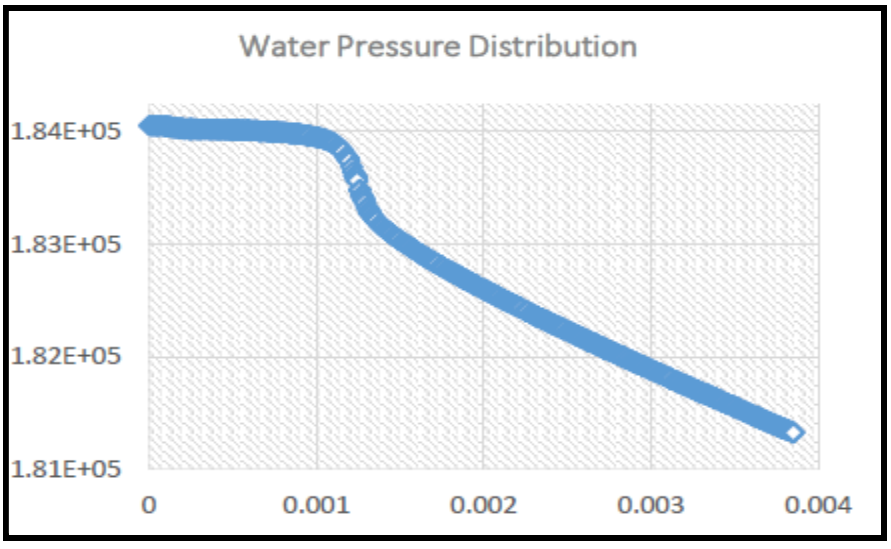

Fig. 17 Pressure plot for water (Newtonian)

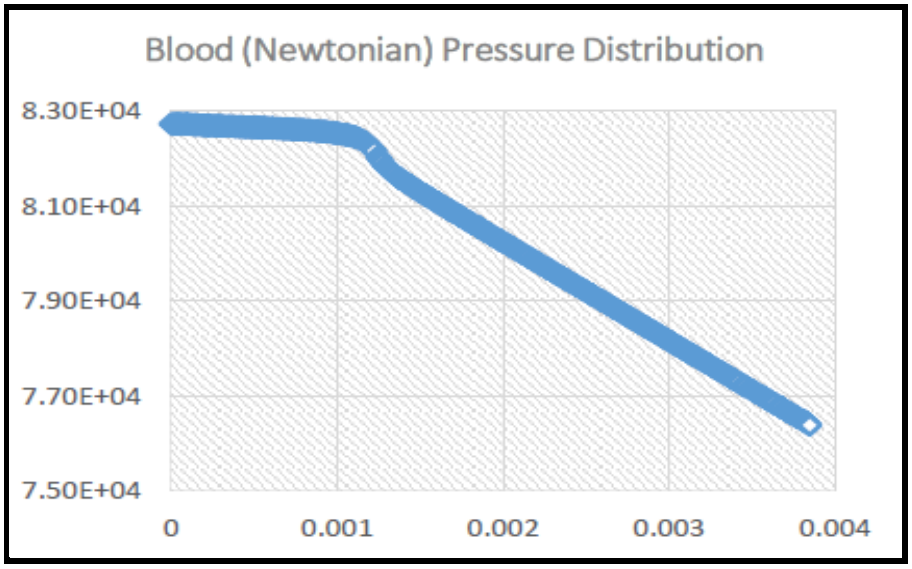

Fig. 18 Pressure plot for blood (Newtonian)

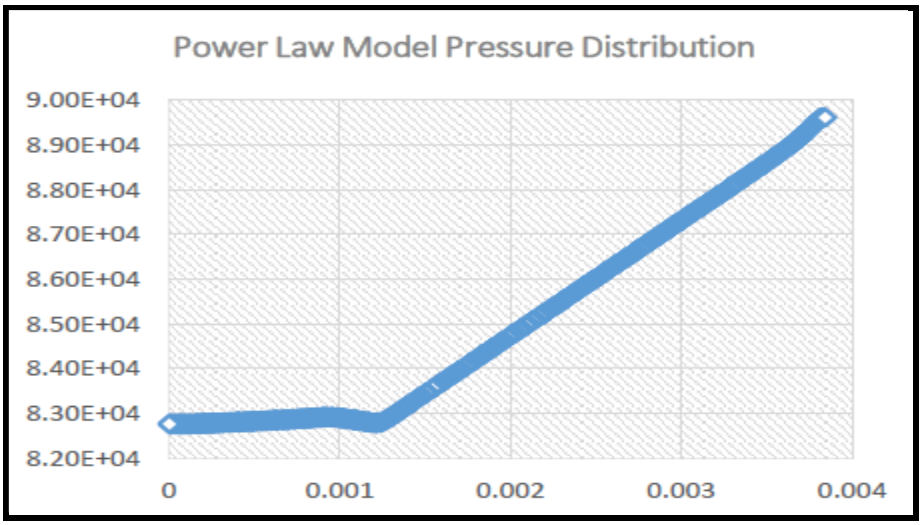

Fig. 19 Pressure plot for blood (power-law non-Newtonian)

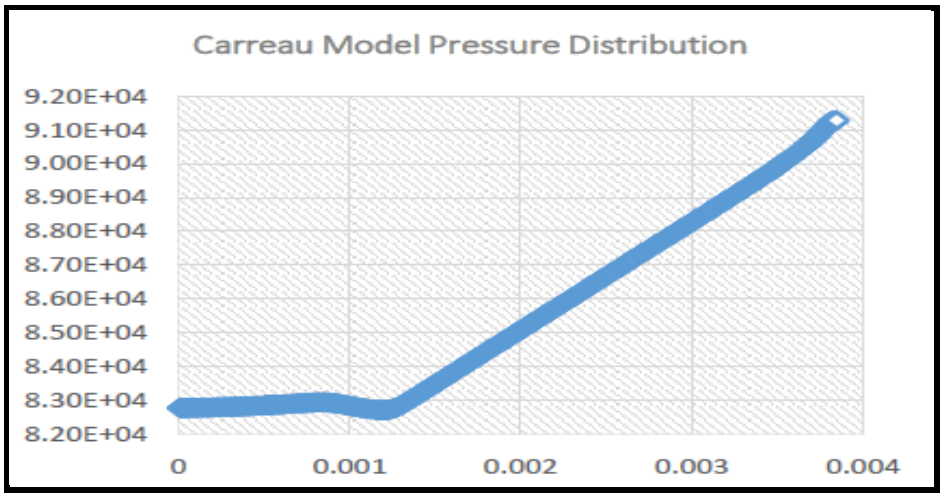

Fig. 20 Pressure plot for blood (power-law non-Newtonian)

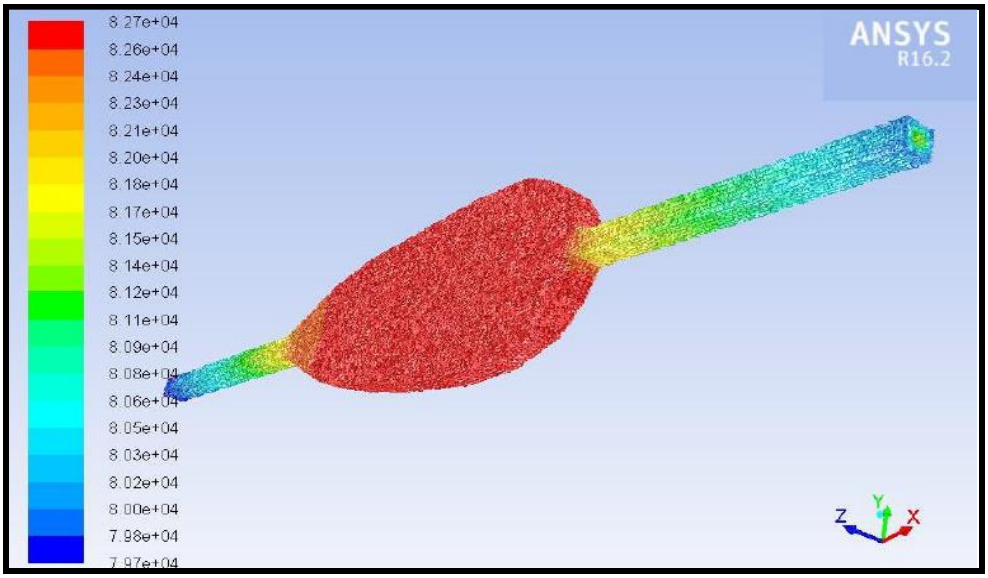

Fig. 21 3-D pressure contour plot for water (Newtonian)

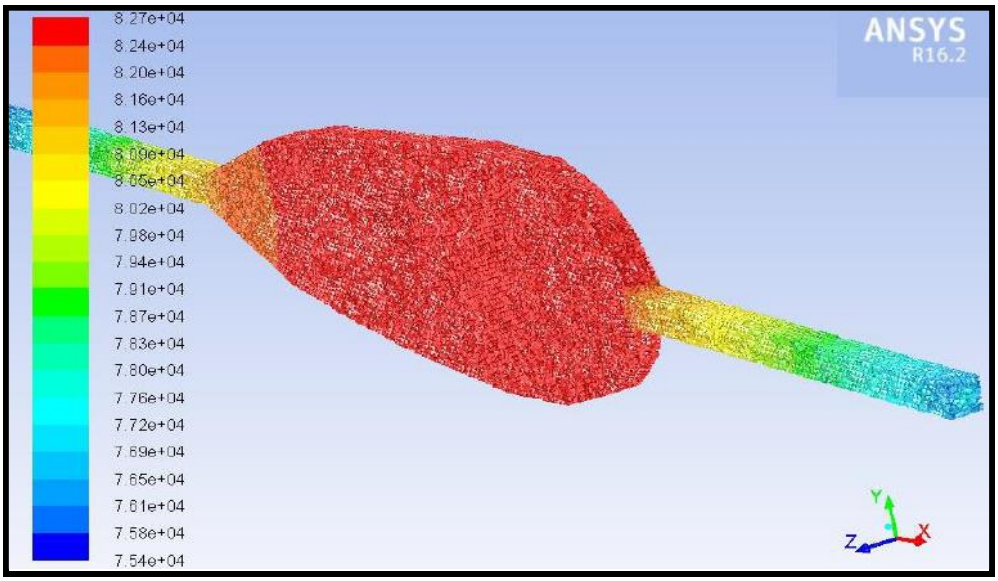

Fig. 22 3-D pressure contour plot for blood (Newtonian)

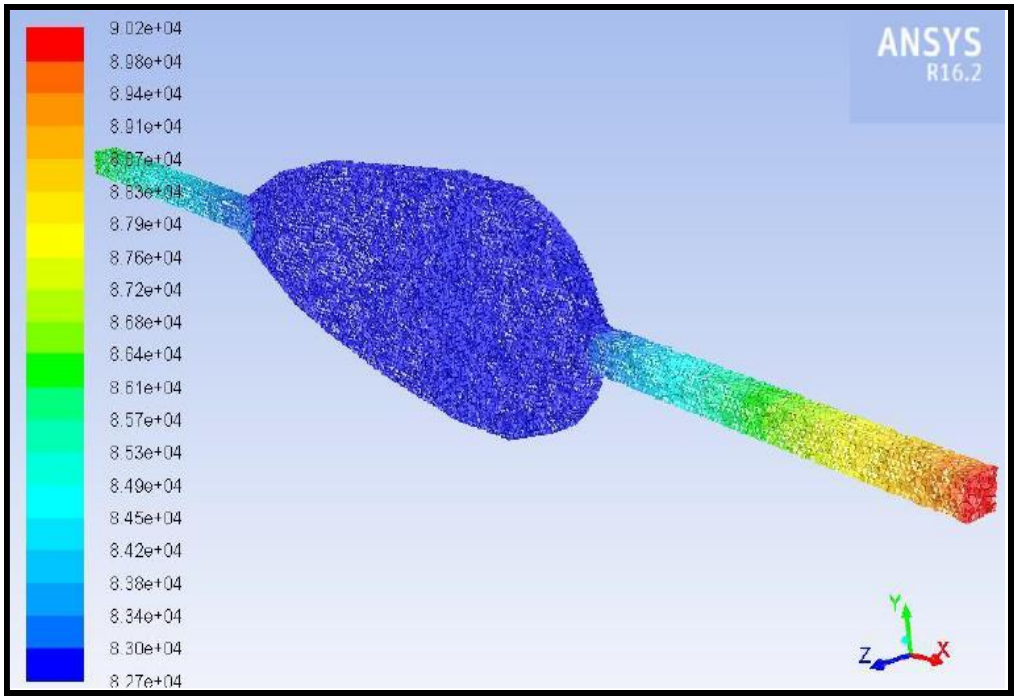

Fig. 23 3-D pressure contour plot for blood (power-law non-Newtonian)

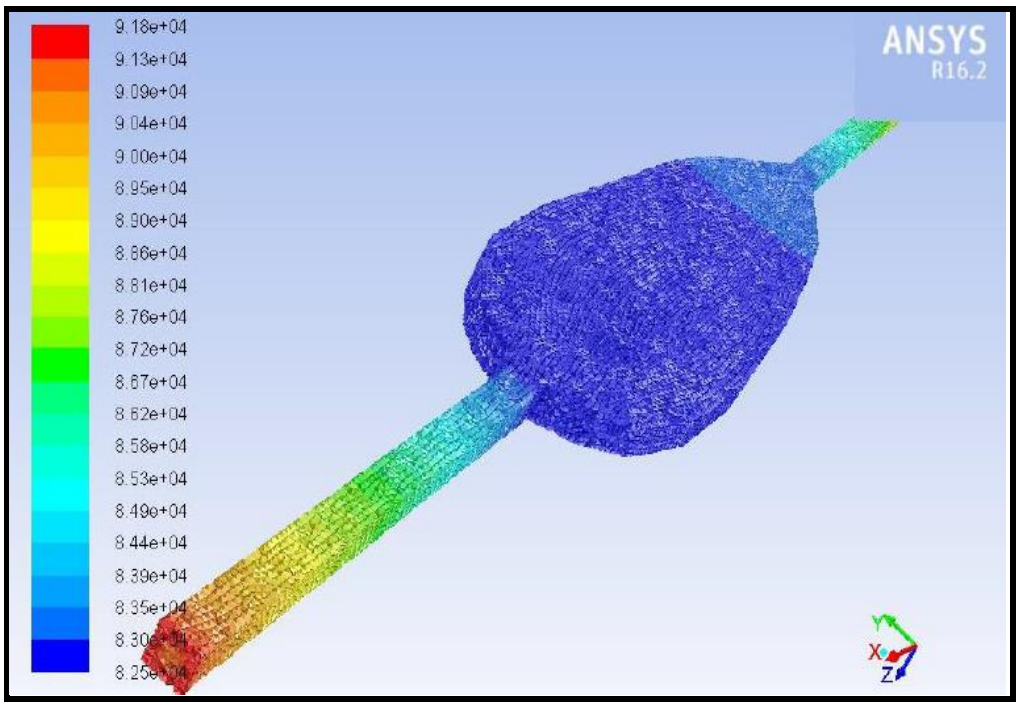

Fig. 24 3-D pressure contour plot for blood (Carreau non-Newtonian)

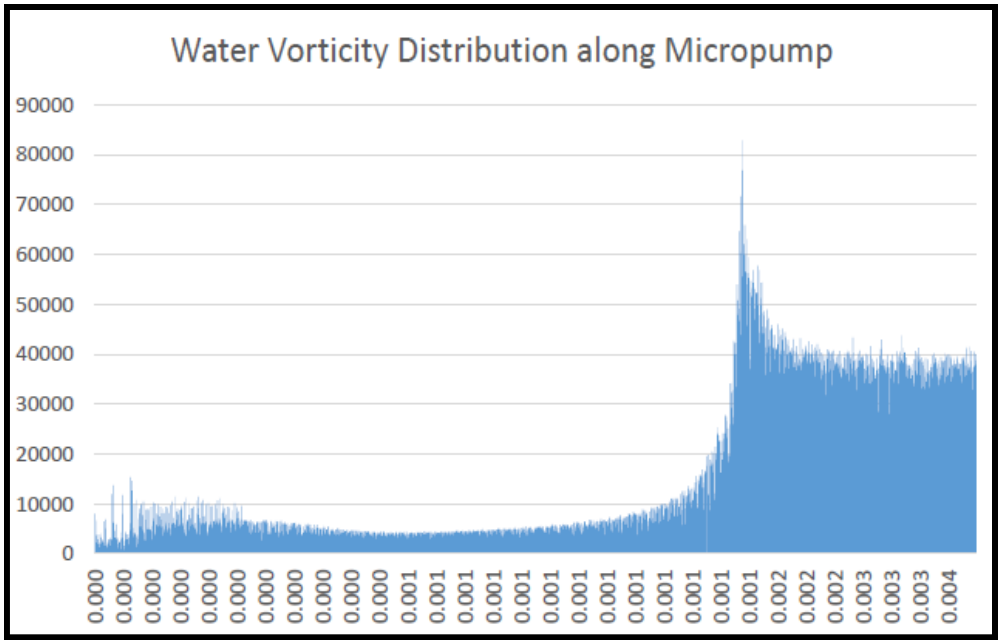

Fig. 25 Vorticity distribution for water (Newtonian)

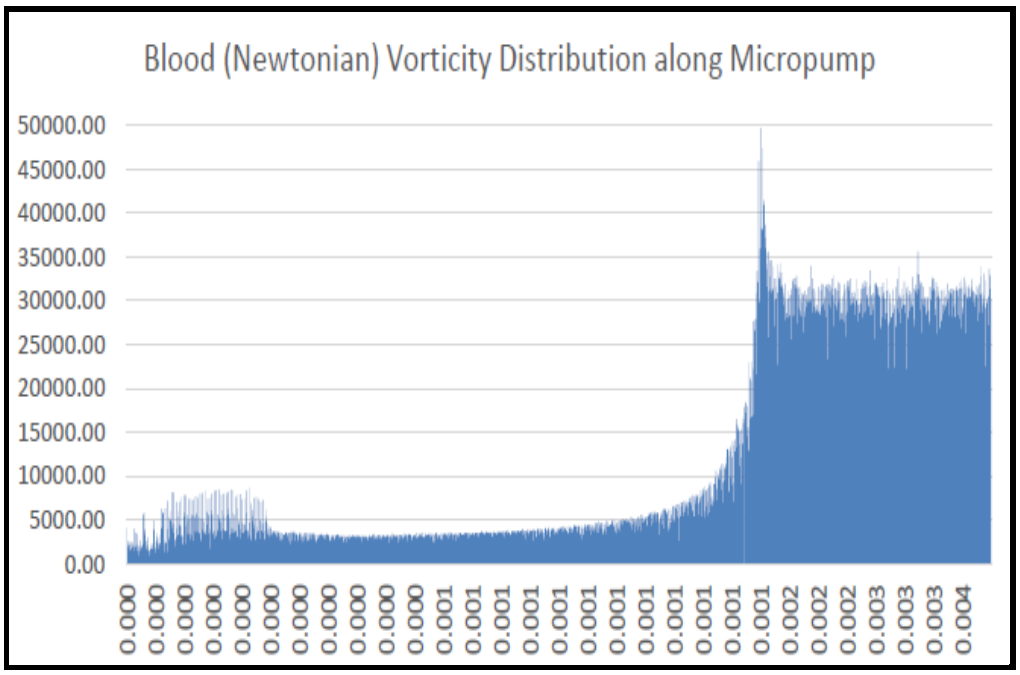

Fig. 26 Vorticity distribution for blood (Newtonian)

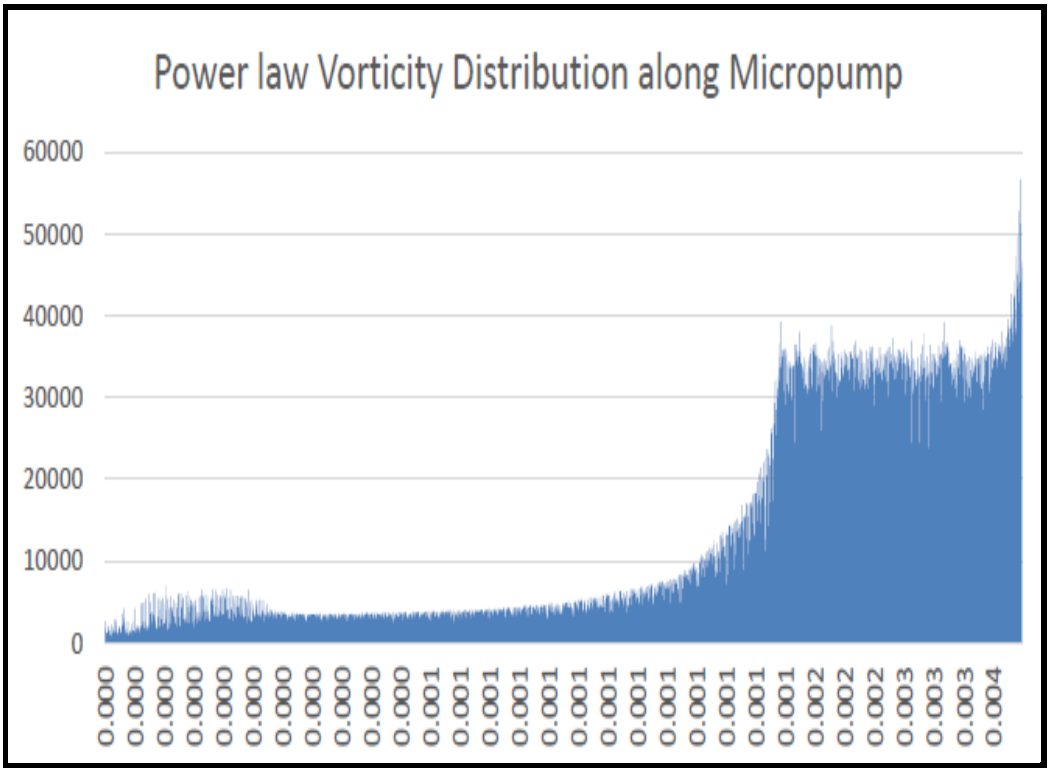

Fig. 27 Vorticity distribution for blood (power-law non-Newtonian)

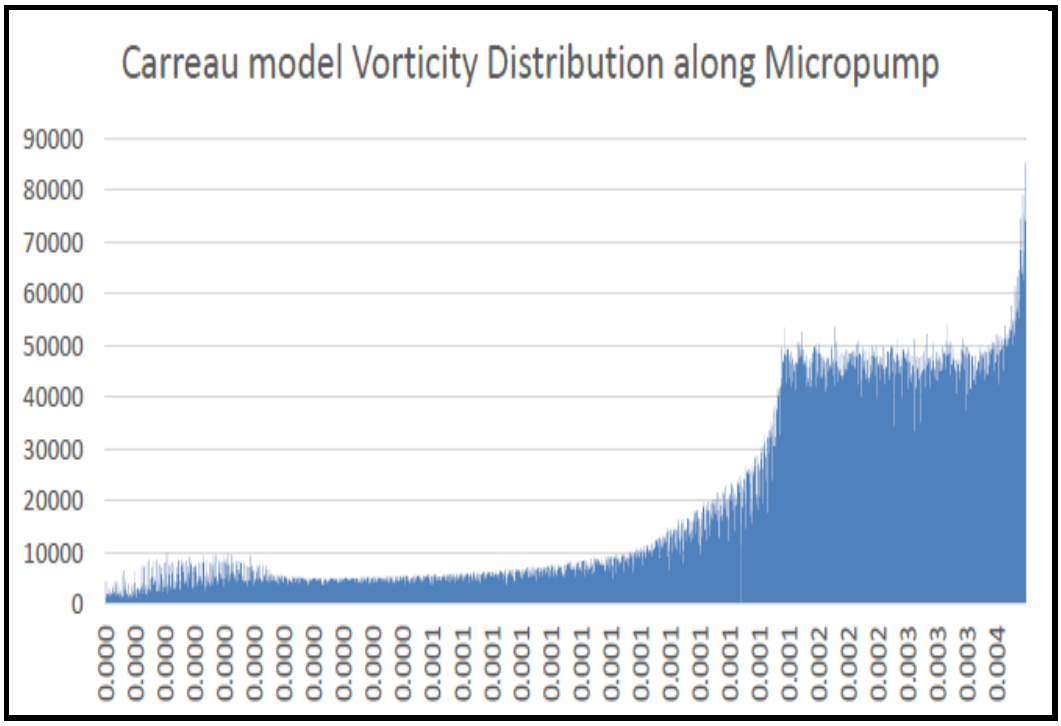

Fig. 28 Vorticity distribution for blood (Carreau non-Newtonian)

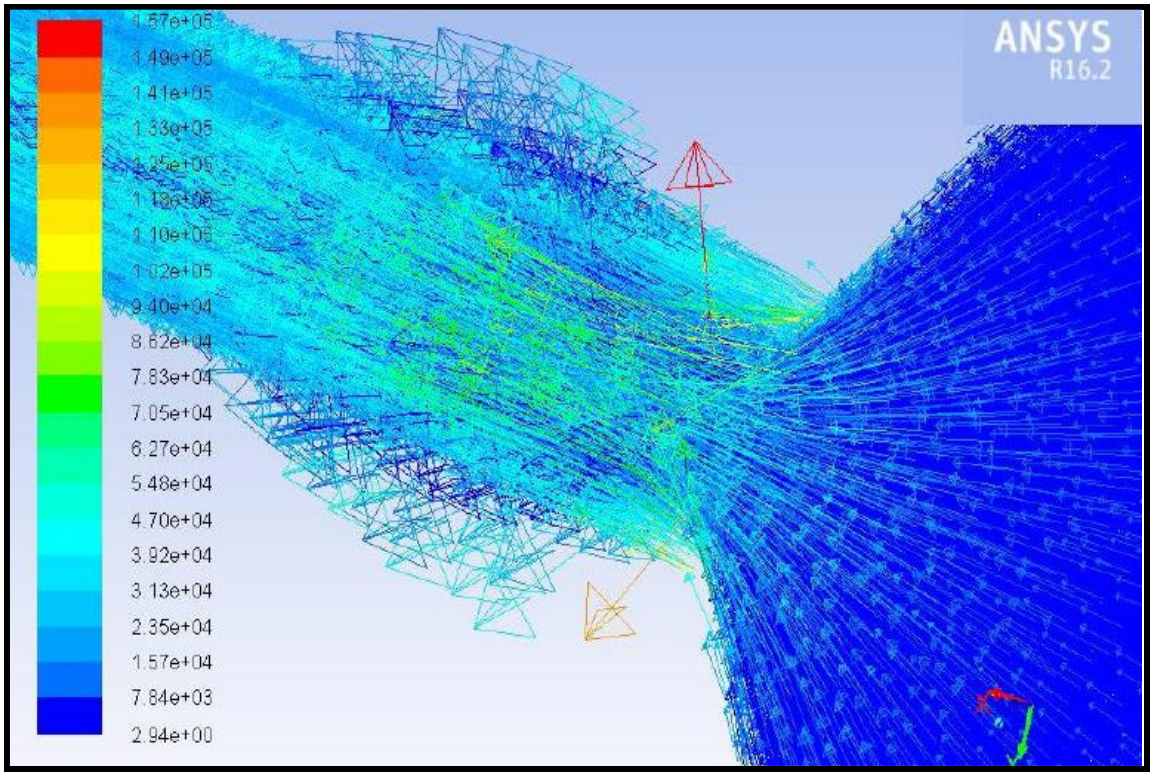

Fig. 29 3-D vorticity contours for water (Newtonian)

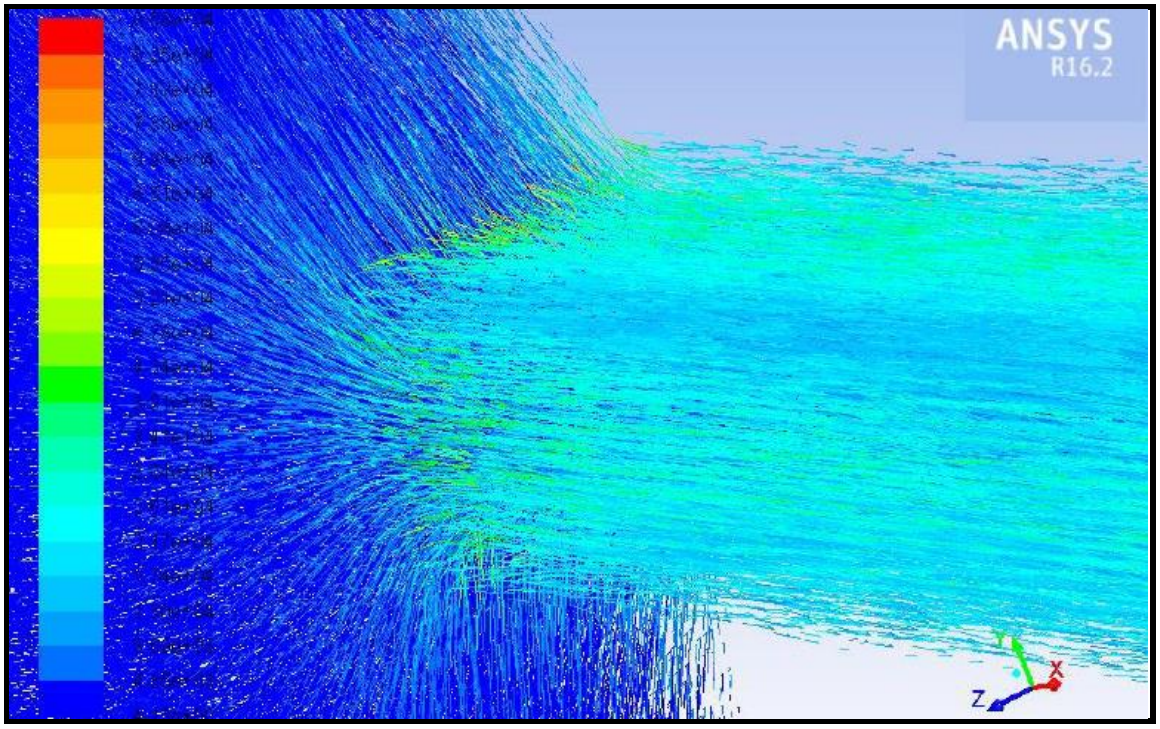

Fig. 30 3-D vorticity contours for blood (Newtonian)

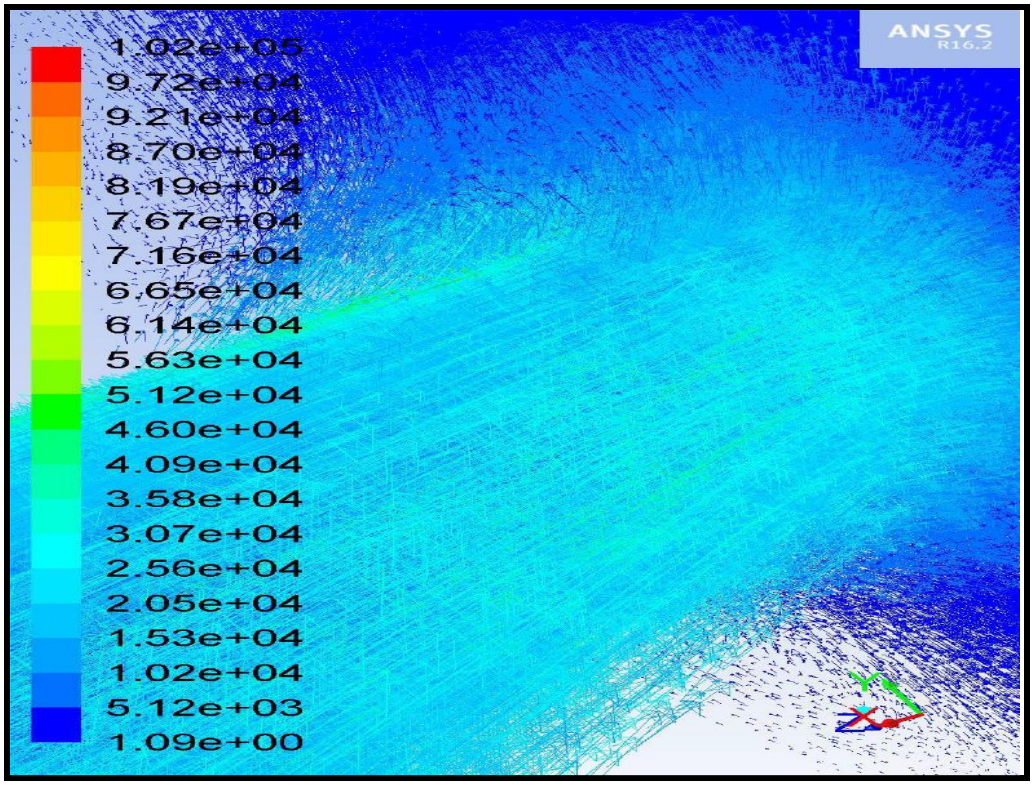

Fig. 31 3-D vorticity contours for blood (power-law non-Newtonian)

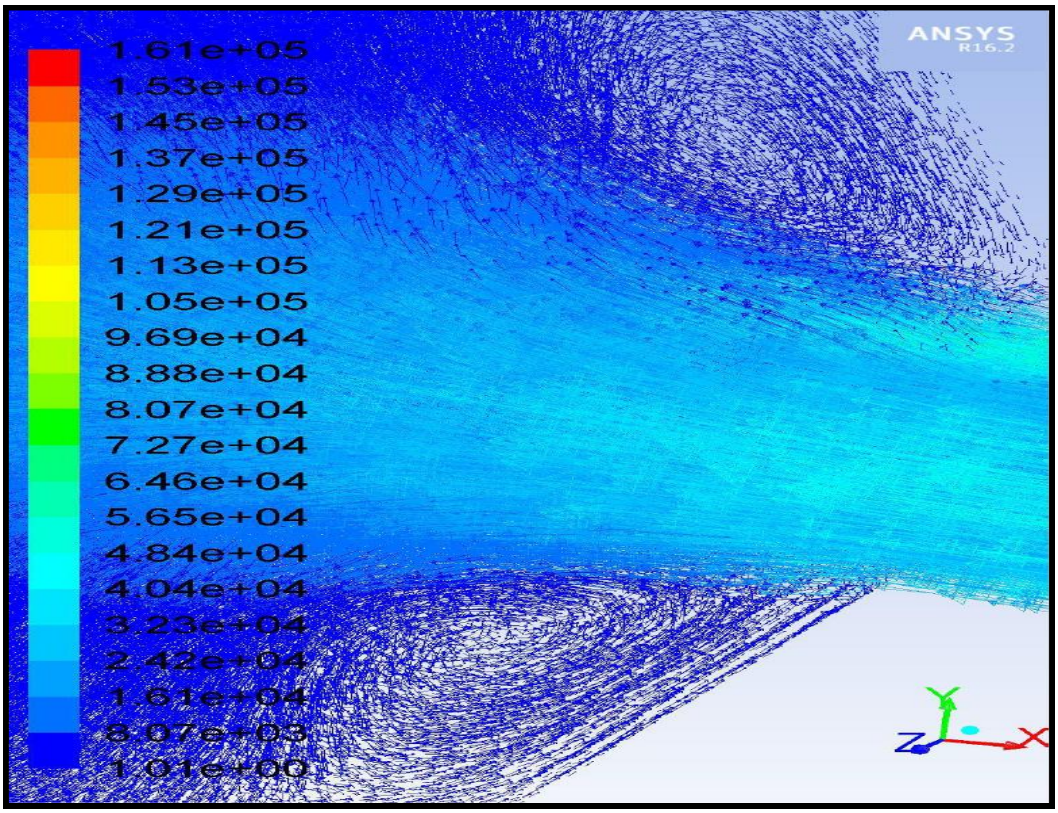

Fig. 32 3-D vorticity contours for blood (Carreau non-Newtonian)

TABLES

Boundary	Condition
Inlet	Pressure -inlet
Outlet 1	Pressure-outlet
Outlet 2	Pressure-outlet
Top wall	Stationary wall with no slip conditions
Bottom wall	Stationary wall with no slip conditions
Side wall 1	Stationary wall with no slip conditions
Side wall 2	Stationary wall with no slip conditions

Table 1 Simulation Boundary conditions

Mesh	Total no. of cells	Total number on Nodes	Velocity at outlet (m/s)	Computational time(minutes)
Double refinement	1114910	204773	1.80382	90
Original mesh	334012	64397	1.795915	20
Half element sizing	143003	28954	1.752749	5
Quarter element sizing	73214	15410	1.715272	2

Table 2: Representation of the effect of mesh density on the simulation values

Pressure (Psi)	Flow rate [2] (µl/s)	Flow rate (µl/s) Present solution (ANSYS Fluent)
0	0	0
2	0.00122	0.0012
4	0.0094	0.00942
6	0.019	0.0188
8	0.025	0.0245
9	0.031	0.030
10	0.036	0.0356
11	0.041	0.0461
12	0.036	0.036

Table 3 Validation results for the simulation